DOI: 10.61782/fa.2025.0637

FORUM ACUSTICUM EURONOISE 2025

NUMERICAL VALIDATION OF VLES-LBM FOR PREDICTING AERODYNAMIC AND ACOUSTIC PHENOMENA IN PROPELLER-WING ULTRA-TIGHT SEPARATION DISTANCES

Lattari, Mateus Grassano[1]*, Beck, Augusto[1]*, Moresco, Luiza Ternes[1]
Silva, Filipe Dutra[2], Salazar, Juan Pablo Lima Costa[2]
Cordioli, Júlio Apolinário[1], Deschamps, César José[1]
[1] Federal University of Santa Catarina, Department of Mechanical Engineering, Florianópolis, Brazil
[2] Federal University of Santa Catarina, Department of Mobility Engineering, Joinville, Brazil

ABSTRACT

eVTOLs and other distributed propulsion aircraft often leverage the benefits of many propellers, resulting in reduced (ultra-tight) propeller-wing separation. Even minor variations in this separation can amplify Blade Passing Frequency (BPF) harmonics and broadband noise, challenging compliance with increasingly stringent noise regulations. To address these concerns, reliable numerical simulations are essential in early-stage aircraft design. In this study, a systematic experimental validation campaign was carried out to confirm the fidelity of simulation results in capturing noise trends under subtle propeller-wing separation changes. PowerFLOW, a high-fidelity aeroacoustics solver, was used to model various propeller-wing separation distances in both the chordwise and spanwise directions, ranging from 10% to 50% of the propeller diameter. The simulations are validated against experimental data for a propeller placed near a NACA 0012 wing inside a semi-anechoic chamber. Time-synchronous analysis of the measured and numerically predicted acoustic noise signals identified the first three BPF harmonics and broadband noise. Amplifications of up to 20 dB in the BPF peaks and up to 10 dB in broadband noise were observed as the separation distance decreased. Overall noise levels and directivity trends from the simulations agreed with measurements within 5–10 dB, which aligns with the expected accuracy for high-fidelity modeling.

**Corresponding author*: *mateus.grassano@polo.ufsc.br.*

Keywords: *Computational Aeroacoustics, Propeller Noise, PowerFLOW).*

1. INTRODUCTION

Distributed electric propulsion (DEP) systems have emerged as promising configurations for future aircraft, offering improved efficiency, reduced emissions, and enhanced design flexibility compared to conventional propulsion systems. These configurations typically feature multiple electric motors with small propellers distributed across the airframe, achieving an integration between propulsion and airframe. While DEP systems present numerous advantages, the close proximity between propellers and wings creates complex aerodynamic interactions. Those interactions can significantly impact both performance and noise emissions. Noise remains a critical concern for urban air mobility (UAM) applications, where stringent noise regulations must be met to ensure community acceptance and operational viability.

Recent investigations reveal that propeller-wing positioning substantially influences aerodynamic performance. Close positioning enhances thrust and lift up to a 30% increase in wing lift and 45% higher thrust when propellers were near the wing trailing edge [1]. Rotorcraft analyses highlight the intricate flow interactions among rotors and wings, underscoring the tight coupling between aerodynamic performance and acoustic outputs in designs where efficient propulsion must balance against community noise requirements [2].

However, propeller-wing proximity simultaneously amplifies acoustic emissions in various manners. Tonal noise increases up to 20 dB at blade passing frequencies [1]. Small adjustments in wing placement significantly affect propeller inflow, with SPL increases of 5 to 12 dB as the wing moves from a factor of 0.5 to 0.75 of the propeller radius [3]. In semi-analytical approaches [4], propeller-wing interactions modify both tonal and broadband noise, with closer propeller-wing separation augmenting noise levels up to 10 dB compared to isolated propeller results.

The complex interplay between aerodynamic forces and acoustic emissions necessitates complementary experimental and computational approaches. Numerical simulations reveal intricate noise generation mechanisms, including tonal and broadband noise with complex directivity patterns [5]. However, computational methods require experimental validation, particularly for tightly positioned propeller-wing configurations where flow physics become increasingly complex. State-of-the-art computational aeroacoustic tools, particularly Lattice Boltzmann Methods implemented in PowerFLOW [6], have demonstrated effectiveness in capturing these phenomena when properly validated, as shown in references [7, 8] for propeller applications.

Considering the complex aerodynamics and aeroacoustic phenomena between a propeller and wing in close vicinity, this study aims to compare numerical results obtained with PowerFLOW to experiments featuring a wing in close proximity to a propeller for various spanwise and streamwise positions. After this point, this work is divided into methodology, results and conclusions.

2. METHODOLOGY

2.1 Method Overview and LBM Formulation

PowerFLOW is a commercial implementation of a LBM solver embedded in hybrid RANS/LES, referred to as Very Large Eddy Simulations (VLES). Lattice Boltzmann (LBM) solvers build upon discretizing the Boltzmann-BGK equation into fixed velocity sets derived from Hermite expansions [9–11]. The collision–propagation scheme is often expressed as:

$$f_a(\mathbf{x} + \xi_a \Delta t, t + \Delta t) = f_a(\mathbf{x}, t) - \frac{1}{\tau}\left[f_a(\mathbf{x}, t) - f_a^{(0)}(\mathbf{x}, t)\right], \quad (1)$$

where f_a is the distribution function, $\mathbf{x}$ is the position vector, ξ_a is the discrete velocity vector, t is time, τ is the relaxation time, and $f_a^{(0)}$ is the equilibrium distribution function.

The method within a hybrid RANS/LES framework is implemented by modifying collision operators with blended relaxation times to incorporate turbulent viscosity. Complex geometries are handled through immersed boundary techniques with fractional cell volumes, while rotating components utilize dynamic meshes with reference frame transformations. Far-field acoustics are computed via the Farassat 1A formulation [12] using pressure and velocity signatures from a cylinder around the propeller and wing system. More details specifically applied to PowerFLOW can be found in [6].

2.2 Numerical Setup and Post-processing

2.2.1 Mesh

Lattice Boltzmann solvers such as the one employed in this research rely on cartesian mesh constructed around the propeller and the wing surface. As mentioned in the previous section, the simulations consider the same geometries as the experimental setup. Special attention were given to the interaction between the propeller wake and the wing. This mesh is constructed with special refinement to the region inside the noise source region. Some special refinements were also made in the propeller tips and trailing edges. The assumptions resulted in converged meshes between 170M to 200M depending on the airfoil-prop distances and 1M timesteps, equivelent to 10 physical propeller rotations.

2.2.2 Boundary conditions

Boundary conditions were constructed in order to mimic the experimental environment, in the boundaries of the computational domain an acoustic absorbing boundary condition is imposed around the propeller in order to capture the anechoic conditions of the experiments. The propeller is embedded inside a rotation cylinder, resulting in a dynamic mesh strategy in order to impose a 5000 RPM rotation.

For correctly predicting the turbulent variables calculated on the propeller surface, a zigzag transitional strip is constructed on the propeller using the same methodology as defined in Reference ([8]).

2.2.3 Post-processing

The next step in post-processing is the signal analysis of the propagated noise. The analysis first relies on Power Density Spectra (PSD) of the propeller noise pressure time signal, calculated in both numerical data and experimental data. For the numerical data, the pressure time signal is obtained through means of the far-field noise propagation. The analysis follows the same microphones defined for the experiment.

In order to evaluate the directivity, results are analyzed in OASPL, but also for signal decomposed BFPs (tonal noise) and broadband. These results are obtained through Time Synchronous Analysis [13].

2.3 Parametric Study

The parametric study is designed to evaluate the effect of the propeller-wing positioning on the noise generated by the propeller, encompassing both numerical simulations and experiments for the same configurations. The propeller and wing are based on an APC 14x10 dual-bladed propeller with a diameter of 300 mm [7] and a NACA 0012 airfoil. Positions are varied spanwisely (Z) and streamwisely (X), as defined in Figures 2a, 2b, and 3a, for spanwise variation and Figures 3a, 3b for streamwise, inclusing Figure 2a.

For the microphones positions considered in this experiments one set of 9 microphones is used. This configurations ranges from angles between -45^o and 45^o , as depicted in Figure 1a. The microphones are placed at a distance of 2 m from the propeller wing system, considering that the microphones are placed on the floor and the propeller is located at 1.6 m from the floor.

Experiments replicated the numerical setup geometries and configurations. Testing occurred in a 5.2 × 5.2 × 3.5 m semi-anechoic chamber (100 Hz cutoff frequency). The propeller-wing system utilized adjustable aluminum profiles, with a T-Motor U3 KV700 and Alpha 40A 6s ESC for propulsion. Measurements were taken using GRAS 46AE microphones and an ATI mini40 load cell, with data acquired through PXIe-4499 boards (National Instruments). Figure 1b shows the complete setup within the chamber.

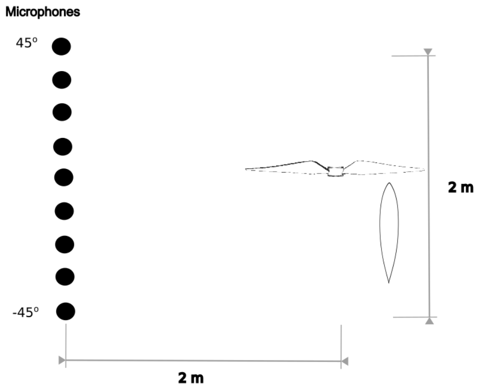

(a) Microphone setup for the experiments. The unshielded array is located at a distance of 2 m from the propeller-wing system.

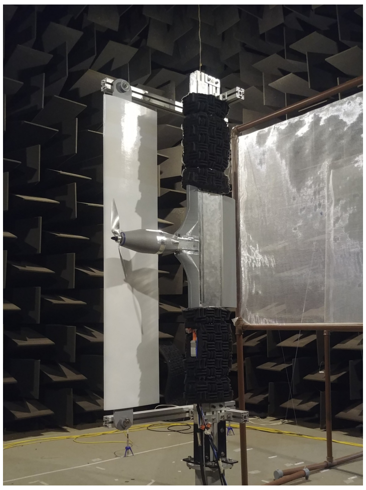

(b) Experimental setup with the propeller and wing in the middle of the semi-anechoic chamber.

Figure 1: Microphone array and experimental setup.

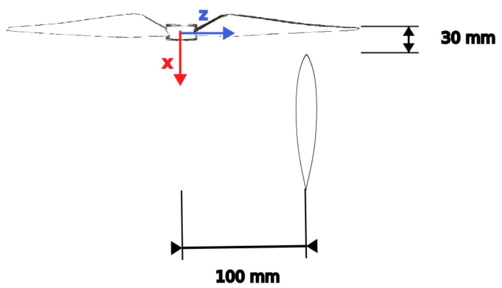

(a) X= - 30 mm, Z=100 mm (2/3 D),

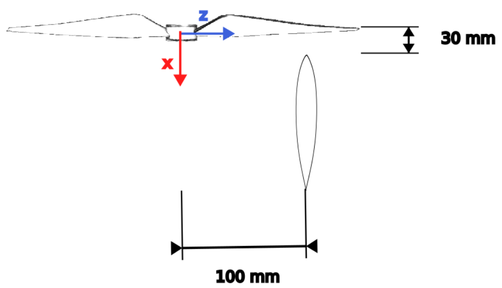

(b) X= - 30 mm, Z=150 mm (3/3 D),

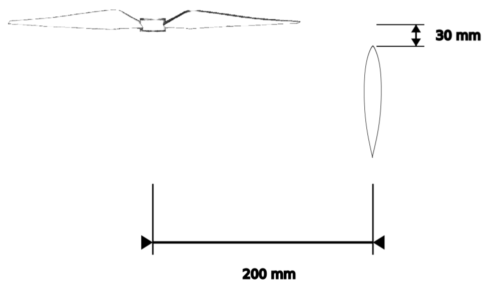

(c) X= -30 mm, Z=200 mm (4/3 D),

Figure 2: Positions of the propeller and wing varied spanwisely with x fixed at -30 mm

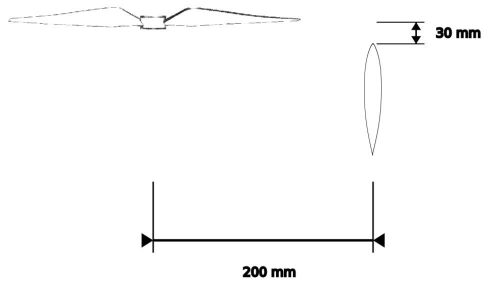

(a) X= -30 mm, Z=200 mm,

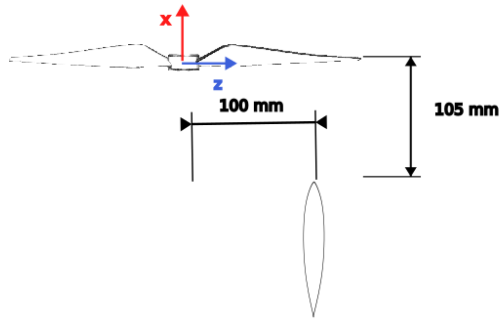

(b) X= -105 mm, Z=100 mm,

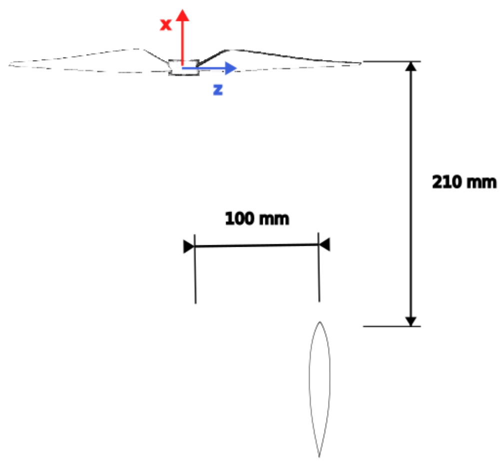

(c) X= -210 mm, Z=100 mm,

Figure 3: Positions of the propeller and wing varied streamwisely with Z fixed at 100 mm

3. RESULTS

3.1 Experimental comparison

Figure 4a compares numerical (lines) and experimental (markes) OASPL directivity for spanwise positions ranging from 100 mm to 200 mm at 5000 RPM at x fixed in -30 mm. The numerical results accurately reproduce both directivity patterns and noise level increments due the reduction of the spanwise Z distance, with absolute differences below 5 dB. Figures 4b–4d present tonal peaks at BPF harmonics. For the first BPF minor variation occurs when Z is reduced from 200 mm to 100 mm, but the simulations are able to obtain the same increment trend as the experimental results. For the second BPF a consistent increment close to 10 dB is observed for each increment, which is captured by the simulations for most of the microphone direction, with an exception for the downstream microphones. A similar trend is observed for the third BPF, but in this case, the simulation seems to have more diffcult to reproduce the trend between a z at 200 mm and 150 mm.

Figures 5a–5d present a similar analysis for streamwise variation (x) of the propeller-wing ranging from -30 mm to 210 mm at z fixed in 100 mm. The same differences between numerical and experimental results are observed, as well as the captured of the noise trends. The exception is the second BPF in x at 105 mm, where for the microphone in -27.5^o, the simulation results seem to diverge from the experimental pattern.

It is important to highlight that in the case of streamwise variation, there is an important increment of the second BPF only when x is modified from -150 mm to -30 mm, close to 20 dB. The BPFs remain almost inaltered when x is varied from 210 to 105 mm.

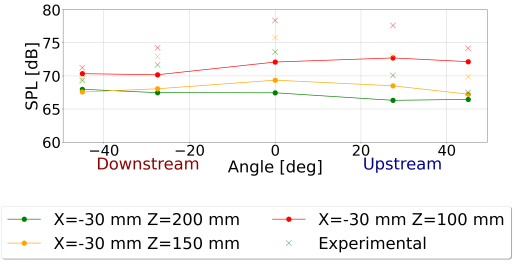

(a) Overall Sound Pressure Level (OASPL).

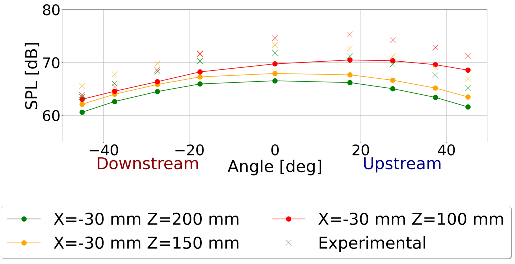

(b) Acoustic tonal contribution at the first Blade Passing Frequency (BPF1) for spanwise variations .

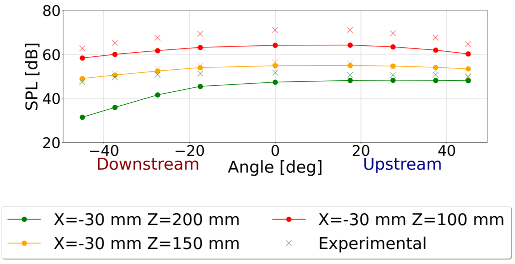

(c) Acoustic tonal contribution at the second Blade Passing Frequency (BPF2) for spanwise variations .

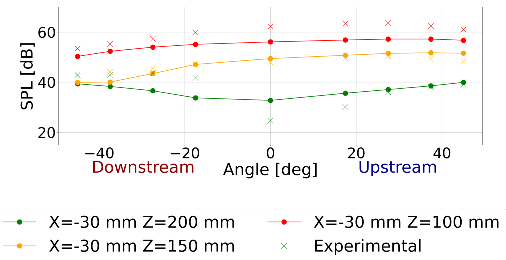

(d) Acoustic tonal contribution at the third Blade Passing Frequency (BPF3) for spanwise variations .

Figure 4: Directivity distribution for the streamwise fixed propeller-wing configurations. Different relative positions of the propeller and wing along the vertical axis are compared.

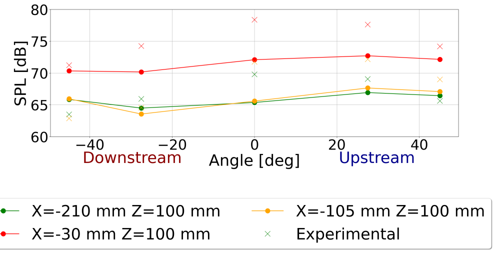

(a) Overall Sound Pressure Level (OASPL).

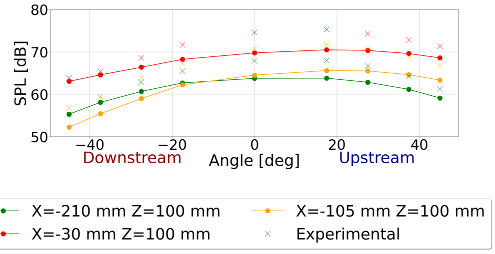

(b) Acoustic tonal contribution at the first Blade Passing Frequency (BPF1) for the propeller-wing arrangement at fixed .

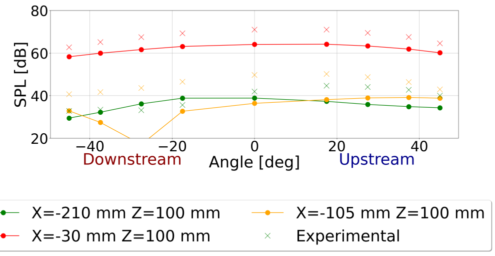

(c) Acoustic tonal contribution at the second Blade Passing Frequency (BPF2) for the propeller-wing arrangement at fixed .

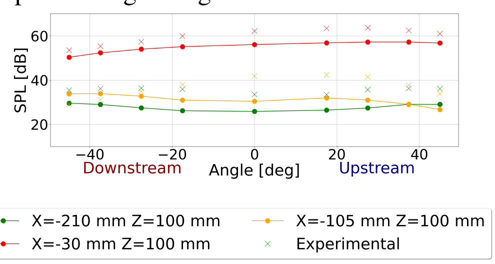

(d) Acoustic tonal contribution at the third Blade Passing Frequency (BPF3) for the propeller-wing arrangement at fixed .

Figure 5: Directivity distribution for the spanwise fixed propeller-wing configuration at fixed . Different relative positions of the propeller and wing along the vertical axis are compared.

4. CONCLUSIONS

In this paper, simulations were validated against experimental results to confirm the fidelity of the numerical results in capturing noise trends under propeller wing distances variation spanwisely and streamwisely. PowerFLOW numerical results for OASPL and BPF peaks ranging from the first to the third BPF, extracted using Time Syncronous Analysis, were compared to measurements.

In temrs of spanwise variations, results showed that the numerical simulations were able to capture the trends of the OASPL and BPF peaks, with differences generally below 5 dB. Important increments in the second and third BPF due to the reduction of the spanwise distance were efectivelly captured by the simulations, with differences below 5 dB. For the streamwise variations, the same trends were observed, with the exception of the second BPF for a propeller-wing distance of 105 mm, where the simulations diverged from the experimental results, specifically for the microphone in -27.5^{o}. In summary, the numerical results were able to capture the trends of the OASPL and BPF peaks, with differences generaly below 5 dB, demonstrating the capability of the numerical simulations to reproduce the experimental results in tightly coupled propeller-wing configurations.

5. REFERENCES

[1] D. A. Giraldo, M. Roger, and M. C. Jacob, “Experimental study of the aerodynamic noise of a pair of pusher-propellers installed over a wing,” in *AIAA Aviation 2023 Forum*, p. 3359, 2023.

[2] T. Stokkermans, L. Veldhuis, B. Soemarwoto, R. Fukari, and P. Eglin, “Breakdown of aerodynamic interactions for the lateral rotors on a compound helicopter,” *Aerospace Science and Technology*, vol. 101, p. 105845, 2020.

[3] N. S. Zawodny, D. D. Boyd, and D. M. Nark, “Aerodynamic and acoustic interactions associated with inboard propeller-wing configurations,” in *AIAA Scitech 2021 Forum*, p. 0714, 2021.

[4] D. C. Akiwate, A. Parry, P. Joseph, and C. C. Paruchuri, “Analytical investigation of propeller-wing interaction noise,” in *28th AIAA/CEAS Aeroacoustics 2022 Conference*, p. 2877, 2022.

[5] A. Vieira, A. Malgoezar, M. Snellen, and D. G. Simons, “Experimental study of shielding of propeller

noise by a wing and comparison with model predictions," *Repository TU DELFT*, 2018.

[6] D. Systèmes, *PowerFLOW 2022-R3 Documentation*, 2023. Version 2021-R4.

[7] D. Casalino, E. Grande, G. Romani, D. Ragni, and F. Avallone, "Definition of a benchmark for low reynolds number propeller aeroacoustics," *Aerospace Science and Technology*, vol. 113, p. 106707, 2021.

[8] G. Romani, E. Grande, F. Avallone, D. Ragni, and D. Casalino, "Performance and noise prediction of low-reynolds number propellers using the lattice-boltzmann method," *Aerospace Science and Technology*, vol. 125, p. 107086, 2022. SI: DICUAM 2021.

[9] X. Shan, X.-F. Yuan, and H. Chen, "Kinetic theory representation of hydrodynamics: a way beyond the navier-stokes equation," *J. Fluid Mech.*, vol. 550, p. 413, 2006.

[10] H. Chen, S. Orszag, I. Staroselsky, and S. Succi, "Expanded analogy between boltzmann kinetic theory of fluid and turbulence," *J. Fluid Mech.*, vol. 519, pp. 301–314, 2004.

[11] R. Zhang, X. Shan, and H. Chen, "Efficient kinetic method for fluid simulation beyond the navier-stokes equation," *Phys. Rev. E*, vol. 74, no. 4, p. 046703, 2006.

[12] F. Farassat, "Derivation of formulation 1 and 1a of farassat," Tech. Rep. TM-2007-214853, NASA, 2007.

[13] R. Randall, *Vibration-based Condition Monitoring: Industrial, Automotive and Aerospace Applications*. Wiley, 2021.